Flow Control by Smart Nanofluidic Channels: A Dissipative Particle Dynamics Simulation

Jianhua Huang,[†,‡] Yongmei Wang,[*,†] and Mohamed Laradji[§]

Department of Chemistry, The University of Memphis, Memphis, Tennessee 38152, Department of Chemistry, Zhejiang Sci-Tech University, Hangzhou 310018, China, Physics Department, The University of Memphis, Memphis, Tennessee 37152-3390, and MEMPHYS−Center for Biomembrane Physics, University of Southern Denmark, DK-5230, Denmark

Received March 21, 2006; Revised Manuscript Received June 5, 2006

ABSTRACT: Dissipative particle dynamics (DPD) simulation is used to investigate solvent flow through a slit channel grafted with stimuli-responsive polymer brushes. The coated channel can regulate solvent permeability when, in response to stimuli, the grafted polymer brush undergoes conformational changes. The effects of the grafting density and the chain length on the flow control capability by the smart channel have been studied. Results show that a nearly 100-fold reduction in permeation rate can be achieved with such smart channels through a proper choice of grafting parameters. Recommendations of suitable grafting parameters for optimum solvent control are given. The interplay between polymer brushes and hydrodynamic flow of the solvent is also briefly revisited. In good solvent regime, the height of the brush with low grafting density decreases with the increase of the pressure drop, but the height of the brush with high grafting density is less perturbed by the pressure drop. In the poor solvent regime, the brush height is even less perturbed by the pressure drop, regardless of the grafting density.

1. Introduction

Porous membranes are used in separation, filtration, catalyst supports, energy storage, drug delivery, and many other applications. Modifications of porous membranes by surface grafting and/or other functionalization techniques are frequently employed to produce tailor-made membranes suitable for specific applications. An interesting class of functionalized porous membranes is stimuli-responsive membranes that are able to regulate fluid and/or solute flow through the membrane in response to changes in environmental variables such as temperature, pH, or the presence of specific chemicals. Such membranes can be fabricated by chemically grafting or coating the pore surface with polymers that can undergo coil-to-globule transition in response to changes in the environmental variables. For instance, poly(acrylic acid)[1] and poly(glutamic acid)[2] undergo such conformational transition in response to pH change, and poly(*N*-isopropylacrylamide) undergoes this transition in response to temperature change.[3] Such polymers, when coated or grafted on the pore surfaces, form layers with a height that is sensitive to the environmental variables. At a good solvent condition, polymers typically swell, resulting in a relatively thick polymer layer. At a poor solvent condition, however, the swelling is reduced and the height of the polymer layer may be substantially reduced. Therefore, a pore grafted or coated with polymers, in a good solvent condition, and with a pore radius comparable to the height of the polymer layer, is clogged. In contrast, in the case of a poor solvent, the polymers are collapsed onto the pore surface, and the pore is open. Permeability of the solvent/solutes through the pore can thus be regulated.

Several groups have recently fabricated such stimuli-responsive membranes with this approach. Park et al.[3] immobilized poly(*N*-isopropylacrylamide), a thermosensitive polymer, on polycarbonate porous membranes, and they found that the rate of water permeation through the immobilized porous membranes changed with temperature while the permeation rate through untreated membranes was independent of temperature. However, the variation in the rate of water permeation, achieved in this study, was small. The same group[3,4] later used gold-coated nanoporous membrane and assembled poly(glutamic acid) (PGA) brushes on the gold surface. A 2-fold reduction of permeation rate is achieved when pH is changed from acidic to alkaline values. PGA is an ionizable polypeptide with its conformations dependent upon pH and ionic strength: At low pH, a PGA chain is protonated and forms an α-helical structure, and at high pH, PGA is deprotonated and adopts an extended random coil structure. The PGA brush changes from a more compact layer to a more stretched and extended layer as the pH increases. More recently, Smuleac et al,[5] using a slightly modified approach, immobilized PGA on poly-carbonate track-etched membranes. They demonstrated that both the rate of water permeation and solute transport through the membrane can be reversibly regulated by pH.

The potential applications of such stimuli-responsive membranes include controlled drug delivery, smart valves, and smart chemical storage/release. One of the important characteristics of these applications is the magnitude of change in solvent/solute permeation rate that can be achieved by these materials. If the polymer layer is formed by end-grafting (i.e., a polymer brush), then this quantity depends on grafting density, chain length, pore size, and solvent quality. The equilibrium structures of polymer brushes at both good and poor solvent conditions have been investigated by means of self-consistent field theory,[6−9] Monte Carlo simulations[10−12] and scaling theories.[13] It is fair to say that a good understanding on the equilibrium structure of polymer brush is achieved at good solvent condition, and perhaps less so at poor solvent condition.[14] Solvent flow through polymer brush has also received significant attention[15−24] and has been a subject of controversy during the past decade.

* Corresponding author. E-mail: ywang@memphis.edu. Telephone: 901-678-2629. Fax: 901-678-3447.
† Department of Chemistry, The University of Memphis.
‡ Department of Chemistry, Zhejiang Sci-Tech University.
§ Physics Department, The University of Memphis, and MEMPHYS−Center for Biomembrane Physics, University of Southern Denmark.

10.1021/ma060628f CCC: $33.50
Published on Web 07/13/2006

In particular, the response of the height of the polymer brush to shear flow was debated. Because of the nonequilibrium nature of these systems, theoretical calculations of solvent flow through a polymer brush are complicated by the interplay between the fluid velocity field and the local polymer composition field. Theoretical calculations of fluid flow through a polymer brush[20,25,26] often use a continuum hydrodynamic equation where the velocity profile is solved using the Brinkman equation[25] with an a priori assumed permeability related to the monomer density profile. The obtained velocity profile has been shown by Milner[20] to be very sensitive on the assumed monomer density profile. In particular, a parabolic density profile of the polymer brush leads to a much greater penetration length into the brush region than a step-function density profile would allow. Although the continuum hydrodynamic formalism is useful for qualitative analysis, the accuracy of the fluid flow characteristics obtained with the continuum approach is not firmly established. Furthermore, the density profile of polymer brushes in poor solvents and the corresponding permeability are not completely understood.[14]

In the present work, we used the dissipative particle dynamics (DPD) approach to investigate solvent flow through a slit grafted with a "smart" polymer brush. DPD is a particle-based mesoscopic simulation scheme that has been shown to predict correct hydrodynamic behavior (i.e., the fluid velocity field obeys the Navier−Stokes equation). Since its original inception,[27] the method has become a popular choice for the study of systems where both Brownian motion and hydrodynamic interactions are important. Several groups have used DPD to study grafted polymer layers under shear flow.[28,29] In particular, the height of the polymer brush under different shear rates and varying solvent quality were examined. Here we focus on the ability of smart slits to regulate solvent flow at different grafting densities, chain length, and hydraulic pressure. We model the external stimulus that triggers the polymer coil-to-globule transition by a change in the solvent quality. The interplay between the local solvent velocity field with the local polymer volume fraction is intrinsically taken into account via DPD. We show that nearly 100-fold reduction in permeation rate can be achieved with such smart channels through a proper choice of grafting parameters. The reported results can be used as a guide to experimental designs of such smart channels. A similar "virtual" investigation of flow control by smart channels, but using molecular dynamics was recently reported.[30] In that study, however, only one grafting density with one chain length was examined.

2. Simulation Details

2.1. Basic DPD Scheme. The DPD approach, was introduced by Hoogerbrugge and Koelman[27] and cast in its present form by Español.[31] In DPD, a number of particles are coarse-grained into a fluid element, thereafter called a dpd-particle. These dpd particles interact via pairwise additive interactions that locally conserve momentum, a necessary condition for a correct description of hydrodynamics.[32] The particles move according to Hamilton's equations

$$\frac{\partial \mathbf{r}_i}{\mathrm{d}t} = \mathbf{v}_i \; m_i \frac{\partial \mathbf{v}_i}{\mathrm{d}t} = \mathbf{f}_i \tag{1}$$

where $\mathbf{r}_i$ and $\mathbf{v}_i$ correspond to the position and velocity of particle i and $\mathbf{f}_i$ is the force acting on the ith particle and m_i is its mass, assumed to be the same for all dpd particles. DPD is further differentiated from molecular dynamics by using a pairwise random and dissipative interactions in addition to the conservative interaction. The net force on the ith particle, $\mathbf{f}_i$, is therefore given by

$$\mathbf{f}_i = \sum_{j \neq i} (\mathbf{F}_{ij}^{(C)} + \mathbf{F}_{ij}^{(D)} + \mathbf{F}_{ij}^{(R)}) \tag{2}$$

where $\mathbf{F}_{ij}^{(C)}$, $\mathbf{F}_{ij}^{(D)}$, and $\mathbf{F}_{ij}^{(R)}$ are the conservative force, dissipative force, and the random force, respectively, acting between particles i and j. The conservative force is soft and repulsive, and is, for simplicity, modeled as a linear function of distance up to a some cutoff distance r_c

$$\mathbf{F}_{ij}^{(C)} = \begin{cases} a_{ij}(1 - r_{ij}/r_c)\hat{\mathbf{r}}_{ij} & (r_{ij} < r_c) \\ 0 & (r_{ij} \geq r_c) \end{cases} \tag{3}$$

where a_{ij} is the strength of the repulsive interaction and depends on the species of particles i and j, $\mathbf{r}_{ij} = \mathbf{r}_i - \mathbf{r}_j$, $r_{ij} = |\mathbf{r}_{ij}|$, and $\hat{\mathbf{r}}_{ij} = \mathrm{r}_{ij}/\mathbf{r}_{ij}$. In our simulations, all lengths are reported in units of the cutoff distance r_c. The unit of a_{ij} is $k_B T/r_c$, k_B is Boltzmann's constant, and T is the system temperature. The dissipative and random forces are given by

$$\mathbf{F}_{ij}^{(D)} = -\gamma w^{D(r_{ij})}(\hat{\mathbf{r}}_{ij} \cdot \mathbf{v}_{ij})\hat{\mathrm{r}}_{ij} \tag{4}$$

$$\mathbf{F}_{ij}^{(R)} = \sigma w^{R}{}_{(rij)} \frac{\theta_{ij}}{\sqrt{\Delta t}} \hat{\mathbf{r}}_{ij} \tag{5}$$

where $\mathbf{v}_{ij} = \mathbf{v}_i - \mathbf{v}_j$ is the relative velocity of a pair of particles, σ is the amplitude of the thermal noise, γ is a friction coefficient, $\theta_{ij}(t)$ is a symmetric random variable satisfying

$$\langle \theta_{ij}(t) \rangle = 0 \tag{6}$$

$$\langle \theta_{ij}(t)\theta_{kl}(t') \rangle = (\delta_{ik}\delta_{jl} + \delta_{il}\delta_{jk})\delta_{t,t'} \tag{7}$$

with $i \neq j$ and $k \neq l$. In eqs 4 and 5, w^D and w^R are continuous functions of distance r and become zero when $r_{ij} \geq r_c$. In eq 5, Δt is the iteration time step. The combined effect of the dissipative and random forces is that of a thermostat. Español and Warren[31] showed that in order for the fluctuation−dissipation theorem to be satisfied at some temperature T, the two weight functions and their prefactors must satisfy the following relationship:

$$w^D(r) = [w^R(r)]^2, \; \sigma^2 = 2\gamma k_B T \tag{8}$$

For simplicity, we took

$$w^D(r) = [w^R(r)]^2 = \begin{cases} (1 - r/r_c)^2 & (r < r_c) \\ 0 & (r \geq r_c) \end{cases} \tag{9}$$

We must note that since, in the present work, we deal with a fluid system at nonequilibrium, the use of dissipative particle dynamics is justified since it has been shown to exhibit correct long large scale and mesoscopic hydrodynamics.[32]

In the present work, we set $\sigma = 3.0(\epsilon^3 m/r_c^2)^{1/4}$ where ϵ sets the energy length scale. All our simulations are performed at $k_B T/\epsilon = 1$ and a fluid number density $\rho = 3.0 r_c^{-3}$. The positions and velocities of the particles are solved using a modified velocity−Verlet algorithm proposed by Groot and Warren,[33] with an integration time step $\Delta t = 0.02\tau$ (unless stated otherwise) with the time scale $\tau = (m r_c^2/\epsilon)^{1/2}$. The values of the interaction parameter a_{ij} measured in units of ϵ/r_cwill be presented subsequently.

2.2. Models of Polymer Grafted Channels. Our simulations are performed in a box of linear dimensions L_x, L_y, and L_z, with periodic boundary conditions applied along the x- and y-

directions. Two planar walls parallel to the *xy*-plane confine the fluid particles within the slit. Each wall is made of four layers of dpd particles that are assembled in a face-centered cubic lattice within a height of $1r_c$. The width of the slit where the fluid particles can sample is $H = L_z - 2r_c$. In principle, fluid particles may penetrate into the walls because of the use of soft conservative force between the wall particles and the fluid particles. However, a sufficiently high number density of wall particles (we used $\rho = 8.0r_c^{-3}$) was found to be sufficient to prevent solvent and polymer particles from penetrating the wall. The wall dpd particles interact with solvent and polymer beads via similar conservative, dissipative and random forces to those between other dpd particles. However, for the sake of computational efficiency, the wall particles are "frozen". The effect of freezing the wall on the fluid flow will be discussed shortly. Linear polymer chains are end-grafted on the first layer of the top and bottom walls. The grafted chain ends were also kept frozen. A polymer chain, is modeled as *N* connected dpd particles, representing *N* statistical segments, linked to each other via a finitely extensible nonlinear elastic (FENE) potential[34]

$$U_{\text{intra}}(r_{i,i+1}) \begin{cases} -\frac{k_F}{2}(r_{\max} - r_{\text{eq}})^2 \ln\left[1 - \left(\frac{r_{i,i+1} - r_{\text{eq}}}{r_{\max} - r_{\text{eq}}}\right)^2\right] & \text{for } r_{i,i+1} < r_{\max} \\ \infty & \text{for } r_{i,i+1} \geq r_{\max} \end{cases} \quad (10)$$

where we choose the equilibrium bond length $r_{\text{eq}} = 0.7r_c$, the maximum bond length, $r_{\max} = 2.0r_c$ and the elastic coefficient $k_F = 40\ \epsilon/r_c^2$. Most of our simulations were performed on a box with $L_x = L_y = 8r_c$ and a slit width $H = 20r_c$, unless stated otherwise. The repulsive parameters of solvent−solvent and polymer−polymer are chosen as $a_{ss} = a_{pp} = 25\epsilon/r_c$. The interaction strength between wall and solvent or polymer particles is set to $a_{ws} = a_{wp} = 8\epsilon/r_c$. The polymer−solvent repulsive interaction a_{ps} is varied in order to model the quality of the solvent. We define a parameter Δa:

$$\Delta a = a_{ps} - \frac{1}{2}(a_{ss} + a_{pp}) \quad (11)$$

When $\Delta a = 0$, the polymer−solvent interaction is the same as the polymer−polymer and solvent−solvent interaction, corresponding to an athermal solvent. A large positive value of Δa results in a strongly repulsive force between solvent and polymer particles, hence a poor solvent. A negative value of Δa, however, results in a net attraction between polymer and solvent particles, hence mimicking a good solvent. Once the composite system is equilibrated for 5000τ, an external force f_x, along the *x*-direction, applied on all solvent particles is switched on, thereby generating a flow along the *x*-direction. The system is then let to run for another $20\,000\tau$. The quantities such as the positions, the velocities of solvents and polymer particles are recorded every 10τ. Uncertainties in the velocities are based on fluctuations in the original simulation data. Uncertainties in other reported quantities are estimated using the error propagation method.

3. Results and discussions

3.1. Coil—Collapse Transition of Polymer Chains in Dilute Solution. The coil-to-globule transition of polymer chains in dilute solution has been a subject of intense experimental, theoretical and computational studies.[35−39] Here, we investigate this transition only to establish the range of solvent parameter, Δa, that needs to be explored. The transition is investigated by monitoring the mean square radius of gyration R_g^2 as a function of solvent quality, where R_g^2 is defined as $\langle R_g^2 \rangle = \langle 1/N \sum_{i=1}^{N} (\boldsymbol{R}_i - \boldsymbol{R}_{\text{cm}})^2 \rangle$, $\boldsymbol{R}_i$ is the coordinate of polymer particle *i*, $\boldsymbol{R}_{\text{cm}}$ is the coordinate of center of mass of the chain and the bracket denotes ensemble average. The final reported R_g value is also averaged over all polymer chains in the box. These simulations were performed in a $20 \times 20 \times 20r_c^3$ cubic box without any walls, and the polymer concentration is kept sufficiently dilute, with a volume fraction of polymer beads around 0.025.

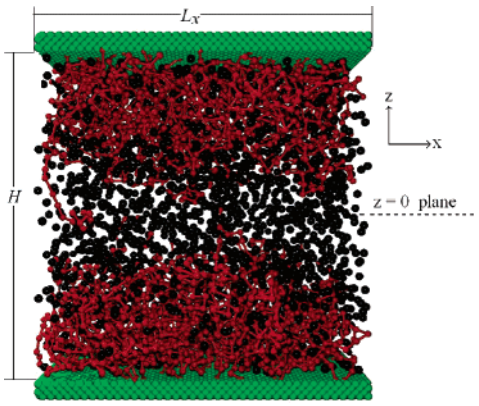

Figure 1. Snapshot of a polymer grafted channel without flow. The grafted polymer chains are red, the wall particles are green and the fluid particles are black. For the sake of clarity, not all fluid particles are shown.

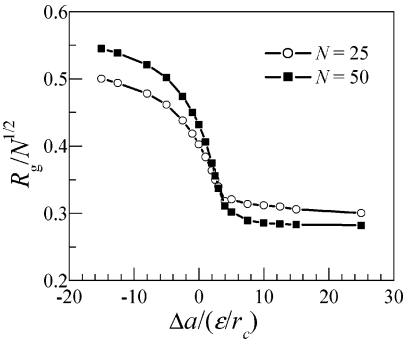

Figure 2. Mean radius of gyration, R_g, of a polymer chain with chain length 25 and 50, as a function of solvent quality parameter Δa.

Figure 2 shows the dependence of the radius of gyration on the solvent quality for two chain lengths. At $\Delta a = 0$, we have confirmed that for $N = 10$ to 100, $R_g \sim N^{\nu}$ with the exponent $\nu = 0.6$, comparing favorably with the expected Flory's exponent for polymers in good solvent. Figure 2 shows that the degree of polymer chains swelling is enhanced as Δa becomes more negative. Although, we did not determine ν for negative Δa, we expect the same value. The Θ point, determined approximately as the point where $R_g/N^{1/2}$ becomes independent of *N*, was found to be around $\Delta a = 3\epsilon/r_c$. The further decrease in R_g as Δa is further increased (in the poor solvent regime) was affected by the clustering of multiple chains in the simulations.

3.2. Poiseuille Flow of Simple DPD Fluid in a Slit. In this section, we present simulation results on Poiseuille flow of simple DPD fluids in a planar channel without grafted polymers. The flow was generated by applying a force f_x on all solvent particles along the *x*-axis. A similar approach was used in the study of flow of an atomistic fluid in a narrow slit by molecular dynamic simulations.[40,41] Due to the soft repulsive interaction between dpd-particles, it is difficult in DPD simulations to build walls that will not have fluid particles penetrating into the walls

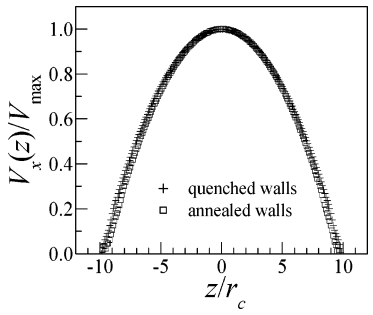

Figure 3. Velocity profiles of a simple DPD fluid confined in a slit with $L_x = L_y = 8r_c$, $H = 19.6r_c$, $f_x = 0.06\epsilon/r_c$ obtained when (+) walls are frozen, (□) walls are annealed. A slip velocity V_{slip} was subtracted from the velocity profile with the frozen walls.

and at the same time no velocity slip near the wall. To get an impenetrable wall, Kong et al.[42] suggested that the density of the wall particles should be four times larger than that in the fluid. This can prevent fluid particles penetrating into the walls, but velocity slip can still occur if the wall particles are frozen. Jones et al.[43] found that the slip was effectively eliminated when a certain velocity was imposed on the fluid particles within a close distance from the wall, even if the density of the wall particles was kept the same as that of fluid. Revenga et al.[44] used an effective force that represented the effect of wall on fluid particles, together with bounce back reflections, to ensure no-slip condition. Using a similar approach, Fan et al.[45] found that simple DPD fluids behave like a Newtonian fluid in Poiseuille flow. However the density fluctuation and temperature drop near the wall still exist. Willemsen et al.[46] added an extra layer of particles, with height equal to the interaction radius, outside the simulation box. The position and velocities of particles in this layer are determined from the position and velocities of particles within the interaction radius of the boundary. Thus, no-slip boundary condition and no density distortion were achieved. However Wijmans et al.[29] found that DPD fluids at a lower density such as $\rho = 3.0r_c^{-3}$ still shows slip at both surfaces.

We compared velocity profiles of Poiseuille flow of DPD fluids in the slit obtained with two different treatments of wall particles. In the first treatment, the wall particles are frozen (quenched walls), and in the second treatment, the wall particles vibrate around their equilibrium lattice points at the same temperature as the fluid particles (annealed walls). In the latter approach, the same conservative, dissipative and random forces described in section 2.1 are applied between wall−wall and wall-fluid particles. The repulsive parameter between wall particles is also set at $25\epsilon/r_c$. The integrity of the lattice is ensured via an anharmonic potential energy anchoring the wall particles to their equilibrium positions, $U(r) = (w_2/2)r_2 + (w_4/4)r^4$, where r is the distance of a wall particle from its respective equilibrium position, and we set $w_2 = 50\epsilon/r_c^2$ and $w_4 = 50\epsilon/r_c^4$. The positions and velocities of wall particles are updated using the leapfrog algorithm with Nose-Hoover thermostat. When the wall is kept frozen, the velocity profile $V_x(z)$ had an appreciable slip near the wall, but after subtracting the slip, it is well-fitted to a parabolic function. For example, for $f_x = 0.06\epsilon/r_c$ and H=19.6r_c, we found $V_x(z) - V_{slip} = (V_{max} - V_{slip})[1 - (z/9.8r_c)^2]$ with $V_{slip} = 3.31(\epsilon/m)^{1/2}$ and $V_{max} = 13.35(\epsilon/m)^{1/2}$. On the other hand, when the wall particles are allowed to vibrate with the same thermal energy (hereafter referred as annealed walls), the velocity profile no longer has the slip and is well-fitted by $V_x(z) = V_{max}[1 - (z/9.8r_c)^2]$ with $V_{max} = 9.51(\epsilon/m)^{1/2}$ at the same conditions. Figure 3 presents the overlap of the two velocity profiles. It is clear that $V_{max} - V_{slip}$ found with quenched walls is slightly larger than V_{max} found with annealed walls under otherwise same conditions. This implies that the effective viscosity of the fluid in the case of annealed walls is slightly larger than that in the case of quenched walls, even after subtracting the slip velocity. This is reasonable since when wall particles are allowed to vibrate, some of the energy will be dissipated through the walls.

We further explore the dependence of the mean fluid velocity along the x-direction, $\langle V_x \rangle$, on the applied force and other parameters with walls kept frozen. For a Newtonian fluid confined in a slit with no-slip boundary condition, the flux generated by a pressure drop ΔP along the x direction is given by

$$Q = \int_0^{Ly} dy \int_{-H/2}^{H/2} dz\, V_x(z) = \frac{Ly\Delta PH^3}{12\eta L_x} \qquad (12)$$

where η is the fluid viscosity. In our simulation, the pressure drop ΔP is generated through the external force f_x applied on the fluid particles. Therefore, $\Delta P/L_x = \rho f_x$. The flux Q is related to the mean velocity $\langle V_x \rangle$ through $Q = \langle V_x \rangle HL_y$. Combined together with eq 12, we obtain $\langle V_x \rangle = \rho f_x H^2/12\eta$. In Figure 4a, $\langle V_x \rangle - V_{slip}$ is shown as a function of the external force f_x for $H = 20r_c$. The linear dependence of $\langle V_x \rangle - V_{slip}$ on f_x is maintained up to $f_x \approx 0.1\epsilon/r_c$. A deviation from the linear dependence is observed at higher values of f_x. This is expected since nonlaminar flow can be produced at high-pressure drop (we estimated a Reynolds number of about 300 when $f_x \approx 0.1\epsilon/r_c$). Figure 4b displays the dependence of $\langle V_x \rangle - V_{slip}$ on the slit width H at a fixed $f_x \approx 0.6\epsilon/r_c$. The data are well-fitted to a power law, $\langle V_x \rangle - V_{slip} \propto H^{1.997\pm0.003}$. In contrast, if V_{slip} is not subtracted, the dependence $\langle V_x \rangle \sim H^2$ is not observed. Figure 4c combines three sets of simulation data on a single plot of $\langle V_x \rangle - V_{slip}$ vs $f_x H^2$. All data collapse on a single linear line. This confirms that we have properly simulated Poiseuille flow of a DPD fluid model in a channel. The presence of a slip velocity at the wall is not a problem as long as it is subtracted from the velocity field. From the slope in Figure 4c, we found an effective viscosity $\eta = 0.887(\epsilon m)^{1/2}/r_c^2$. Though the viscosity of a simple DPD fluid at the same conditions was not found in the literature, our value compares well with those reported after adjusting for the difference in the used parameters. For example, Fan et al.[45] reported a viscosity $\eta = 1.007(\epsilon m)^{1/2}/r_c^2$, but they used a number density $\rho = 4.0r_c^{-3}$ whereas we used $\rho = 3.0r_c^{-3}$. Since the simulation with annealed walls is very time-consuming, the remaining of the study was performed with frozen walls.

3.3. Demonstration of Flow Control Capability of Smart Channels. Section 3.1 shows that polymer chains undergo a coil-to-globule collapse transition when the solvent quality is changed from good to poor. When such polymer chains are grafted to the inner surfaces of a channel at relatively high grafting density, they form a brush with a height that is sensitive to the solvent quality. This in turn can control the solvent flow through the channel. Here we demonstrate the capability of flow control by such smart channels. The channel is grafted with polymer chains with length $N = 25$ at a grafting density $\omega = 0.50r_c^{-2}$ on each wall, where $\omega = N_p/L_xL_y$ and N_p is the number of polymer chains grafted on each wall. We can calculate the reduced surface density, $\Sigma = \pi R_{g0}^2\omega = 3.69$, where R_{g0} is the radius of gyration of a chain with length $N = 25$ in a dilute bulk solution at $\Delta a = 0$. The reduced surface density is a measure of distance between the grafted chains compared with the size of free chains in solutions. If $\Sigma > 1.0$, then the average distance between the grafted chains is greater than the size of the free chains. As a result, the grafted chains are stretched

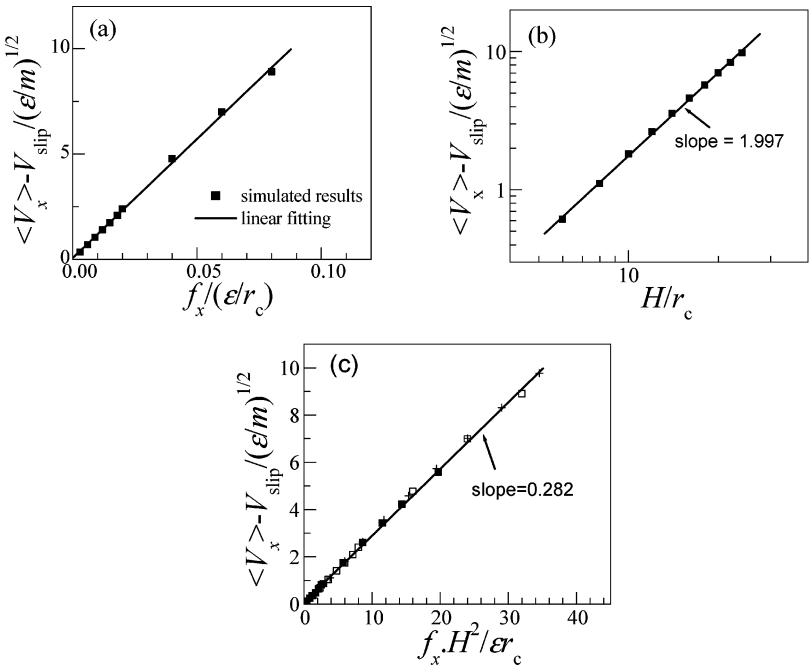

Figure 4. (a) Dependence of $\langle V_x \rangle - V_{slip}$ on the external force, $L_x = L_y = 8r_c$, $H = 20r_c$. (b) log−log plot of $\langle V_x \rangle - V_{slip}$ vs the slit width H, $L_x = L_y = 8r_c$, $f_x = 0.06\epsilon/r_c$. (c) Linear dependence between $\langle V_x \rangle - V_{slip}$ and f_xH^2. Data shown correspond to (□) $L_x = L_y = 8r_c$, $H = 20r_c$, varying f_x; (■) $L_x = 20r_c$, $L_y = 8r_c$, $H = 20r_c$, varying f_x; and (+) $L_x = L_y = 8r_c$, $f_x = 0.06\epsilon/r_c$, varying H.

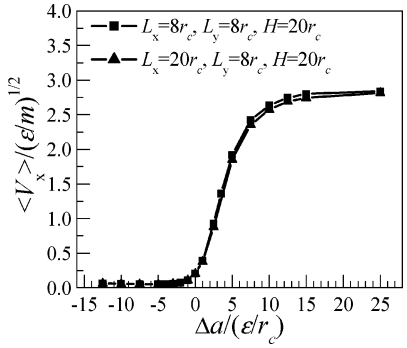

Figure 5. Dependence of the mean solvent velocity on the solvent quality under an external driving force $f_x = 0.06\epsilon/r_c$. $N = 25$, and $\omega = 0.50r_c^{-2}$. Dimensions of the slit channel are given in the figure.

perpendicular to the surface and form brushes. The mean velocity and velocity profile in the channel is obtained after the flow has reached steady-state. Figure 5 shows the dependence of the mean velocity on the solvent quality with a slit of height $H = 20r_c$ in two different box sizes and $f_x = 0.06\epsilon/r_c$. A sharp transition in the mean velocity, from nearly zero to a maximum value of about $2.8(\epsilon/m)^{1/2}$, is observed when the solvent quality changes from good to poor. This figure also shows that finite size effects are minimal. In Figure 6, snapshots of polymer brushes at three solvent conditions are shown. Note that due to shear induced by solvent flow next to stationary walls, the polymer chains are tilted, and that the tilting is enhanced as the solvent quality is reduced. From the snapshots in Figure 6, we clearly observe the slit change from "closed" state to "open" state when the solvent changes from good to poor. At good solvent condition, solvent particles penetrate the polymer layer leading to a swelling of the brushes. However, since the polymers are grafted to the stationary walls, the flow of the solvent is practically blocked due to the frictional drag created by the polymers. We note that the volume fraction of polymer particles in the channel is ∼40% and remains constant when the solvent quality is varied. When the solvent is poor, solvent particles are depleted from the brush region toward the central region of the channel, and the solvent flows mainly through the region devoid of polymers in the middle of the channel. Figure 7 displays the density profiles and velocity profiles of solvent particles along the *z*-axis. When the solvent is poor ($\Delta a = 5$), the solvent density profile is nearly a step function, being constant at $\rho = 3r_c^{-3}$ in the middle of the channel and drops sharply to a lower value at $z \approx \pm 6r_c$, presumably the location of interface between the solvent and the polymer-rich layer.

To quantify the capability of the smart channel to control solvent flow, we define a dimensionless parameter $\kappa = Q/Q_0$, called permeability of the channel, where Q and Q_0 are the flow rates through the channel with and without grafted polymer brushes, respectively, under the same flow conditions. The flow rate Q is proportional to $\langle V_x \rangle$ without subtracting any slip since the velocity field drops to zero continuously in the brush region. However, we used $\langle V_x \rangle - V_{slip}$ for Q_0. In Figure 8, the permeability vs the solvent quality is shown. We note that the permeability is nearly zero for good solvent conditions and approaches 0.40 as the solvent quality is reduced. The latter value is comparable with the ones reported by Adiga and Brenner[30] in their molecular dynamic simulations of smart nanofluidic channels. The permeability in the athermal solvent reported in their study is slightly less than 0.05, also comparable with our value at Δa=0. However, the solvent quality in their study was not varied continuously as in our study. As a result, the change in the permeability in their study[30] does not appear as dramatic as in our simulations. The grafting density ω in their study is $0.01\sigma_{mm}^{-2}$, where σ_{mm} is the diameter of Lennard-Jones particles used in their simulations. Unfortunately, we could not find the corresponding radius of gyration of the chain grafted on the wall in their study, so we are unable to make a quantitative comparison with their systems.

3.4. Effect of Tunable Parameters of Smart Channels on Flow Control. In the design of such smart channels, the tunable parameters include, among others, the surface grafting density and the chain length. Figure 9 shows the effect of surface grafting density on the solvent-sensitive permeability of the

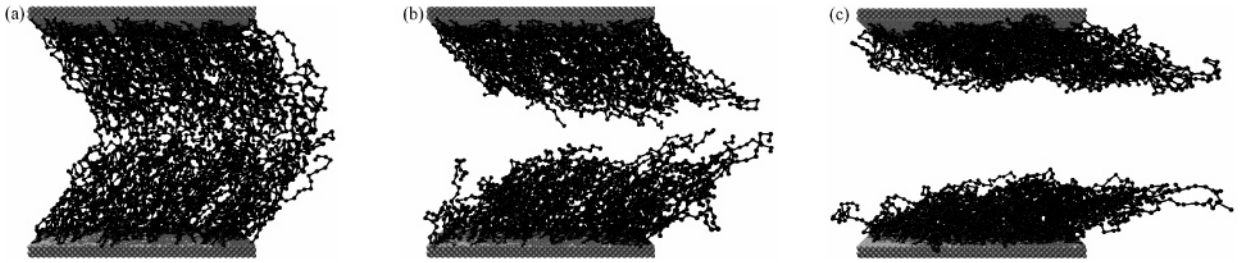

Figure 6. Snapshots of polymer brushes for three values of solvent quality, and under a driving force $f_x = 0.06\epsilon/r_c$. Here, a, b, and c correspond to $\Delta a = -5\epsilon/r_c$, $\Delta a = 0$, and $\Delta a = 5\epsilon/r_c$, respectively. For the sake of clarity, the solvent particles are omitted. Other parameters correspond to $L_x = 20r_c$, $L_y = 8r_c$, $H = 20r_c$, $N = 25$, and $\omega = 0.50r_c^{-2}$.

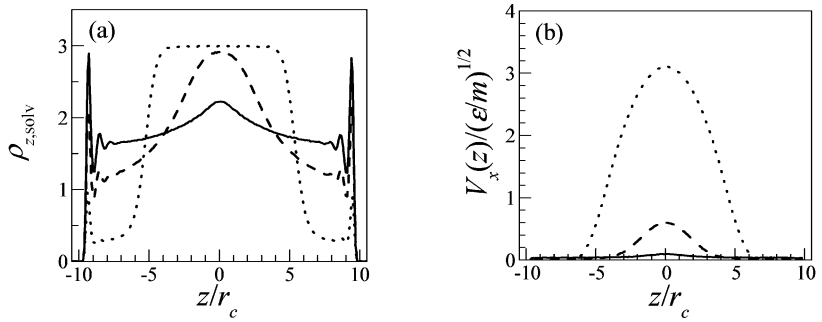

Figure 7. Solvent density profiles (a) and velocity profiles (b) at different solvent qualities Δa, corresponding to those in Figure 6. Key: (−) $\Delta a = -5\epsilon/r_c$; (- -) $a = 0$; (•••) $a = 5\epsilon/r_c$.

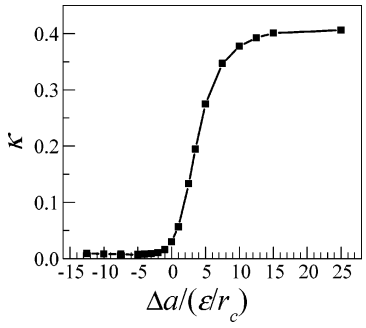

Figure 8. Permeability through a slit channel with width $H = 20r_c$ as a function of the solvent quality. The grafting density $\omega = 0.5r_c^{-2}$ and chain length $N = 25$.

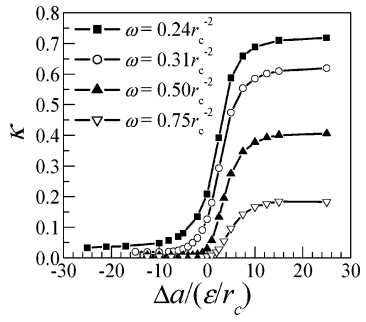

Figure 9. Permeability as a function of solvent quality at different grafting densities for $N = 25$, $L_x = L_y = 8r_c$, and $H = 20r_c$.

smart valve. We note from this figure that independently of the solvent quality, the channel permeability is reduced as the grafting density is increased. However, the absolute change in the permeability κ as ω is varied is more significant in the poor solvent condition (open state) than in good solvent condition (closed state). When the grafting density $\omega = 0.50r_c^{-2}$, the permeability of the channel in the good solvent condition is as low as 0.0035 (also, see data in Table 1). Further increase in the grafting density significantly reduces the permeability of the channel in the poor solvent condition. At a smaller grafting density, such as $\omega = 0.24r_c^{-2}$, although the permeability in the open state is large, there is an appreciable permeability in the closed state. When the grafting density is too small, the channel leaks even in the closed state and the control of the flow may not be effective.

Table 1. Characteristics of Solvent Control by Smart Channel at Different Grafting Densities (Slit Channel Width $H = 20r_c$ and Grafted Chain Length $N = 25$)[a]

ωr_c^2	Σ	κ_{min} ($\times 10^{-2}$)	κ_{max}	Δa_c	hillslope α	$\kappa_{max}/\kappa_{min}$	$\kappa_{max} - \kappa_{min}$
0.24	1.77	4.55	0.714	2.23	0.204	15.7	0.667
0.31	2.28	1.90	0.608	2.79	0.228	32.0	0.589
0.50	3.69	0.35	0.394	3.71	0.274	111	0.391
0.75	5.55	0.22	0.179	5.03	0.281	82.3	0.177

[a] Uncertainties of the data are in the last digit of the reported numbers.

For the ease of analysis, the sigmoidal dependence of κ on solvent quality Δa in Figure 9 was fitted to the dose response curve with variable slopes, used frequently in the study of drug pharmacology.[47] Namely

$$\kappa = \kappa_{min} + \frac{\kappa_{max} - \kappa_{min}}{1 + 10^{\alpha(\Delta a_c - \Delta a)}} \tag{13}$$

where κ_{min}, κ_{max} are the minimum and maximum permeability, respectively, α is the hillslope, and Δa_c is the solvent quality when $\kappa = (\kappa_{max}\text{-}\kappa_{min})/2$. We will refer to Δa_c as the crossover point from the open to the closed states. Table 1 summarizes the fitting parameters obtained at the four different grafting density along with the corresponding reduced surface densities Σ. For the four systems investigated, the reduced surface densities Σ are all greater than one. The four systems studied here are well in the brush regime.[48] At moderate grafting densities such as $\omega = 0.31r_c^{-2}$ and $0.50r_c^{-2}$, the crossover point Δa_c is close to the estimated θ-solvent condition, $\Delta a_c \approx 3.0\epsilon/r_c$. At high grafting densities, the crossover point Δa_c shifts toward conditions with poorer solvent quality. At high grafting densities, densely grafted polymers have to stretch away from the surface due to excluded-volume interactions between

Table 2. Characteristics of Solvent Control by Smart Channel with Different N and H at a Fixed Grafting Density $\omega = 0.50 r_c^{-2}$

N and H/r_c	Σ	κ_{min} ($\times 10^{-2}$)	κ_{max}	Δa_c	a	$\kappa_{max}/\kappa_{min}$	$2L_{max}/H$
$N = 10, H = 20$	1.08	23.4	0.744	0.961	0.126	3.18	0.630
$N = 25, H = 20$	3.69	0.35	0.394	3.71	0.274	111	1.68
$N = 50, H = 20$	8.87	0.22	0.0468	8.33	0.279	21.3	3.43
$N = 25, H = 18$	3.69	0.41	0.336	4.19	0.284	82.0	1.87
$N = 25, H = 14$	3.69	0.53	0.270	5.64	0.270	50.9	2.40

monomers. Consequently, the channel is not effectively open unless the solvent is very poor. This observation is in accord with the experimental reports.[49] The hillslope α is a measure of the steepness of the response curve. A large α corresponds to a steeper response. As the grafting density increases, α increases slightly. Our results indicate that a smart channel with densely grafted brushes produces a somewhat sharper transition response than a channel with low grafting densities.

Important indicators of performance characteristics of smart channels must depend on specific types of applications. The ratio, $\kappa_{max}/\kappa_{min}$, should serve as one of these performance indicators. The data in Table 1 clearly shows that $\kappa_{max}/\kappa_{min}$ reaches a maximum at the grafting density $\omega = 0.50 r_c^{-2}$ (or $\Sigma = 3.69$) and that a further increase in the grafting density leads to a decrease in this ratio. The difference $\kappa_{max} - \kappa_{min}$ decreases with increasing grafting density. At $\omega = 0.24 r_c^{-2}$, which is the lowest grafting density investigated here, the difference, $\kappa_{max} - \kappa_{min}$, is largest. However, it is foreseeable that this difference may decrease with a further reduction in the grafting density. Limited simulations at even lower grafting density (data were not included in Table 1) confirmed this conjecture.

Table 2 compares the control characteristics of smart channels with different chain lengths and slit widths for a given grafting density. The polymers in these systems are again in the brush regime, indicated by the reduced surface density Σ being greater than one. We also added to Table 2 another indicator, $2L_{max}/H$, where L_{max} is the contour length of the grafted polymer chain and is calculated as $L_{max} = (N - 1)r_{eq}$ where $r_{eq} = 0.7 r_c$ is the equilibrium bond length. L_{max} serves as measure of an upper limit of the brush height (bond stretching beyond the equilibrium bond length can occur but is negligible in most cases) when the grafting density reaches the maximum. When $2L_{max}/H \sim 1$, then fully extended brushes will clog the pore at good solvent condition. Although the range of the parameters, $2L_{max}/H$ and Σ, investigated here is limited, we can clearly see that when $2L_{max}/H < 1$, there is an appreciable permeability through the channel in the closed state (e.g., for $N = 10$, $H = 20 r_c$, $\kappa_{min} = 0.234$). If $2L_{max}/H$ is large (e.g., $2L_{max}/H > 2.0$), we find that the permeability in the open state becomes small (e.g., for $N = 50$, $H = 20 r_c$, $\kappa_{max} = 0.0468$). Increasing $2L_{max}/H$ from 1.68 to 2.40 at fixed $\Sigma = 3.69$ (see data in Table 2) lowers the ratio $\kappa_{max}/\kappa_{min}$ from 111 to 50.9. From limited data in Tables 1 and 2, we can conclude that the two grafting parameters, Σ and $2L_{max}/H$, have a range of values during which the ratio $\kappa_{max}/\kappa_{min}$ will reach maximum. The smart channel will have the optimum control of solvent flow. The exact ranges for Σ and $2L_{max}/H$ are still unknown and they may mutually depend on each other. Current limited data suggest that $2L_{max}/H$ should be between 1 and 2 and Σ needs to be at least greater than 1.0 but a further increase of Σ beyond an optimum value will degrade the performance of the smart channel.

3.5. Interplay between Solvent Flow and Brush Height. Finally, we present in this section simulation results on the interplay between solvent flow and brush height. The shear response of polymer brushes under good solvent conditions, due to solvent flow, has been the subject of considerable debate during the past decade.[15−17,19,21−25,28,29,50−53] Earlier studies suggested that shear lead to swelling of polymer brushes.[17,22,24,25] However, later experiments[23,53] and computer simulations[19,28,29] have shown that brushes do not swell under shear. In fact, simulations have indicated there is a reduction in the brush height at high shear rate owing to the stretching of the chains along the shear direction.[19,21,29] X-ray and neutron reflectivity studies on the effects of solvent flow on the height and density profile of a polymer brush revealed no change in either quantity for a range of shear rates.[23,53] Here we show that this conclusion holds true in the poor solvent regime. We calculated the brush height using the first moment of the brushes:[10]

$$h = \frac{1}{2}\sum_{k=1}^{2} \frac{\int_{-H/2}^{H/2} dz\, |H/2 - z| \rho_k(z)}{\int_{-H/2}^{H/2} dz\, \rho_k(z)} \qquad (14)$$

where $\rho_k(z)$ is the density profile of a polymer layer k and $z = 0$ corresponds to the middle of a slit of height H. Parts a and b of Figure 10 compare the brush heights at different shear rates at two grafting density. For small grafting densities, we observe a decrease in the brush height with the increase of the shear rate (i.e., as f_x is increased) in the good solvent regime, but in the poor solvent regime the shear force has little effect on the brush width. The observed response of the brush width to the shear rate in good solvent conditions is consistent with results reported in recent simulation studies.[29] Wijman et al.[29] also observed that the reduction in the brush width with the increase of shear rate is more significant when the grafting density is low. For low grafting densities, the amount of solvent in the polymer brush is appreciable, and as we have seen earlier, the slit is not completely closed. Therefore, the polymer chains experience shear stresses caused by the solvent flow. Since the polymer chains remain stationary, the net force acting on them along x-axis is zero. The shear stresses are compensated by polymers stretching along the x-axis. At higher grafting densities, the solvent is more stationary in the polymer layer than at low grafting densities. Therefore, the polymer layer does not experience much shear stresses due to solvent flow, and the polymer brush becomes practically unaffected by the flow rate. Our simulations further show that brush width is very insensitive to the shear rate in the poor solvent regime. When the solvent is poor, solvent particles are fairly excluded from the polymer layer. Consequently, the flow has very little effect since the height of the polymer brushes is essentially determined by the incompressibility condition.

The permeability through channels coated with polymer brushes was reported to depend on the shear rate or the hydraulic pressure drop. Experimentally Castro et al.[54] reported an increase in the permeability with the shear rate through a polymer grafted microporous silica membrane. They attributed this increase to the reduction in the brush width at high shear rate. More recently, Adiga and Brenner[30] investigated the permeability of cylindrical channels coated with polymer brushes in an athermal solvent for different force. Their simulations results showed a correlation between the increase of the permeability rate and the decrease in the brush height, as the shear rate increases. We have only investigated two different values of driving force, $f_x = 0.06\epsilon/r_c$ and $0.137\epsilon/r_c$. We note that latter value is slightly above the range over which a Poiseuille flow holds in the absence of polymers. Nevertheless, the increase in the permeability at high shear force is clearly seen. More interestingly, the increase of the permeability is more appreciable in the poor

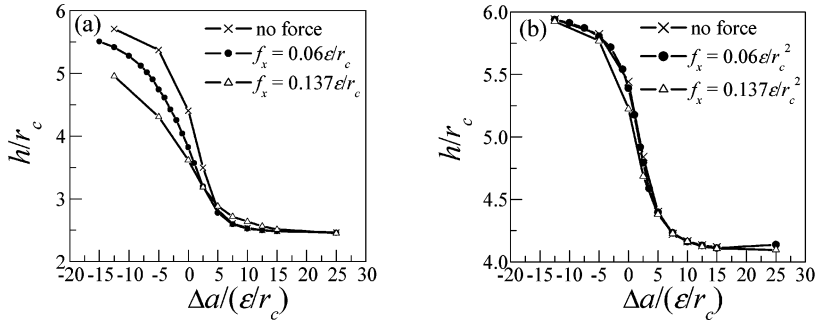

Figure 10. Effect of the driving force, f_x, on the first moment of the polymer brushes, h, at two grafting densities (a) $\omega = 0.31r_c^{-2}$ and (b) $\omega = 0.75r_c^{-2}$.

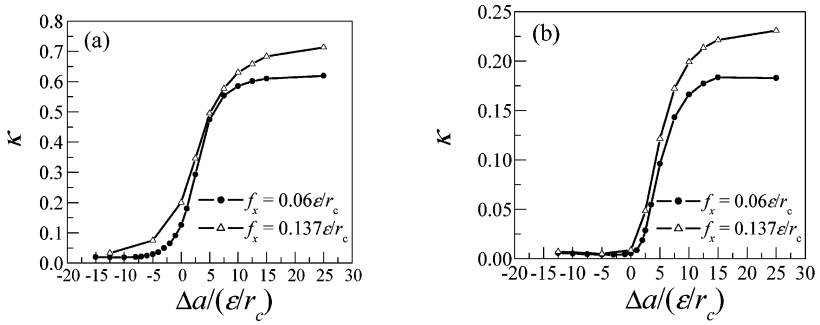

Figure 11. Effect of the driving force, fx,on the permeability (at two different grafting densities corresponding to to (a) $\omega = 0.31r_c^{-2}$ and (b) $\omega = 0.75r_c^{-2}$.

solvent regime than in the good solvent regime (see Figure 11). In the poor solvent regime, however, the brush width is not significantly affected by the driving force of the flow (see Figure 10). These findings suggest that the increase in the permeability with the increase of shear force may not entirely come from the reduction in the brush height, as proposed by Castro et al.[54] One of the possible reasons is that the solvent velocity profile in the coated channel does not entirely fit to a parabolic function. The velocity profile has a tail that slowly drops to zero in the brush region. The extent of this tail is modulated by the interaction of the solvent particles with the brush, which is influenced by the solvent quality and the driving force. The presence of a slowly decaying tail in the velocity profile when polymer brushes are present implies that the velocity profile is not parabolic (Poiseuille flow), and therefore $\langle V_x \rangle$ need not be proportional to the driving force f_x. More investigations at other values of f_x are needed to characterize solvent flow through coated brushes.

4. Concluding Remarks

Dissipative particle dynamics (DPD) method is employed to investigate solvent flow through a slit channel grafted with "smart" polymer chains. DPD is more suitable for the investigation than coarse grained molecular dynamic simulations. We show in this study that Poiseuille flow of simple PDP fluids in a slit channel without grafted polymer layers is properly simulated even when the wall particles are frozen. When the wall particles are frozen, the velocity profile had an some slip near the walls, but after subtraction of the slip, the velocity profile is well fitted to a parabolic function. The dependence of the mean velocity, after subtraction of the slip, on the applied force and the slit width conforms to the Poiseuille law. The capability of smart channels to control solvent flow is demonstrated in the study. A nearly 100-fold reduction in the permeation rate can be achieved with such smart slits through a proper choice of grafting parameters.

In the current study, we focused on the solvent control capability by the smart channel. The interplay between polymer brushes and hydrodynamic flow of the solvent is only briefly investigated, since this topic has received significant attention before. Under good solvent conditions, we observed a decrease in the brush height with the increase of the shear rate at low grafting density. This agrees with earlier reported simulation results.[29] Under poor solvent conditions, the brush height is found to be very insensitive to the shear rate.

Acknowledgment. This work was supported by a research fund made available by The University of Memphis. M.L. acknowledges support from the donors of the Petroleum Research Fund, administered by the American Chemical Society, and The University of Memphis Faculty Research Grant. The latter support does not necessarily imply endorsement by the university of research conclusions.

References and Notes

(1) Ito, Y.; Park, Y. S.; Imanishi, Y. *J. Am. Chem. Soc.* **1997**, *119*, 2739−2740.
(2) Ito, Y.; Ochiai, Y.; Park, Y. S.; Imanishi, Y. *J. Am. Chem. Soc.* **1997**, *119*, 1619−1623.
(3) Park, Y. S.; Ito, Y.; Imanishi, Y. *Langmuir* **1998**, *14*, 910−914.
(4) Ito, Y.; Park, Y. S.; Imanishi, Y. *Langmuir* **2000**, *16*, 5376−5381.
(5) Smuleac, V.; Butterfield, D. A.; Bhattacharyya, D. *Chem. Mater.* **2004**, *16*, 2762−2771.
(6) Milner, S. T.; Witten, T. A.; Cates, M. E. *Macromolecules* **1988**, *21*, 2610−2619.
(7) Milner, S. T. *J. Chem. Soc., Faraday Trans.* **1990**, *86*, 1349−1353.
(8) Zhulina, E. B.; Borisov, O. V.; Birshtein, T. M. *J. Phys. (Paris) II* **1992**, *2*, 63−74.
(9) Zhulina, E. B.; Borisov, O. V. *J. Chem. Phys.* **1997**, *107*, 5952−5967.
(10) Laradji, M.; Guo, H.; Zuckermann, M. J. *Phys. Rev. E* **1994**, *49*, 3199−3206.
(11) Lai, P. Y.; Zhulina, E. B. *J. Phys. (Paris) II* **1992**, *2*, 547−560.
(12) Wijmans, C. M.; Scheutjens, J. M. H. M.; Zhulina, E. B. *Macromolecules* **1992**, *25*, 2657−2665.
(13) Halperin, A.; Zhulina, E. B. *Macromolecules* **1991**, *24*, 5393−5397.
(14) Binder, K. *Eur. Phys. J. E* **2002**, *9*, 293−298.
(15) Rabin, Y.; Alexander, S. *Europhys. Lett.* **1990**, *13*, 49.
(16) Klein, J.; Perahia, D.; Warburg, S. *Nature* **1991**, *352*, 143−145.
(17) Kumaran, V. *Macromolecules* **1993**, *26*, 2464−2469.
(18) Lai, P.-Y.; Lai, C.-Y. *Phys. Rev. E* **1996**, *54*, 6958−6961.

(19) Miao, L.; Guo, H.; Zuckermann, M. J. *Macromolecules* **1996**, *29*, 2289−2297.
(20) Milner, S. T. *Macromolecules* **1991**, *24*, 3704−3705.
(21) Lai, P. Y.; Binder, K. *J. Chem. Phys.* **1993**, *98*, 2366−2375.
(22) Barrat, J. L. *Macromolecules* **1992**, *25*, 832−834.
(23) Baker, S. M.; Smith, G. S.; Anastassopoulos, D. L.; Toprakcioglu, C.; Vradis, A. A.; Bucknall, D. G. *Macromolecules* **2000**, *33*, 1120−1122.
(24) Harden, J. L.; Cates, M. E. *Phys. Rev. E.* **1996**, *53*, 3782−3787.
(25) Sevick, E. M.; Williams, D. R. M. *Macromolecules* **1994**, *27*, 5285−5290.
(26) Wu, D. T.; Cates, M. E. *Macromolecules* **1996**, *29*, 4417−4431.
(27) Hoogerbrugge, P. J.; Koelman, J. M. V. A. *Europhys. Lett.* **1992**, *19*, 155-.
(28) Irfachsyad, D.; Tildesley, D.; Malfreyt, P. *Phys. Chem. Chem. Phys.* **2002**, *4*, 3008−3015.
(29) Wijmans, C. M.; Smit, B. *Macromolecules* **2002**, *35*, 7138−7148.
(30) Adiga, S. P.; Brenner, D. W. *Nano Lett.* **2005**, *5*, 2509−2514.
(31) Espanol, P.; Warren, P. *Europhys. Lett.* **1995**, *30*, 191−196.
(32) Ripoll, M.; Ernst, M. H.; Espanol, P. *J. Chem. Phys.* **2001**, *115*, 7271−7284.
(33) Groot, R. D.; Warren, P. B. *J. Chem. Phys.* **1997**, *107*, 4423−4435.
(34) Kremer, K.; Grest, G. S. *J. Chem. Phys.* **1990**, *92*, 5057.
(35) Wu, C.; Zhou, S. *Macromolecules* **1995**, *28*, 8381−8387.
(36) Wang, X.; Qiu, X.; Wu, C. *Macromolecules* **1998**, *31*, 2972−2976.
(37) Wang, X.; Wu, C. *Macromolecules* **1999**, *32*, 4299−4301.
(38) Hu, T.; You, Y.; Pan, C.; Wu, C. *J. Phys. Chem. B* **2002**, *106*, 6659−6662.
(39) Lai, P.-Y. *Macromol. Theor. Simul.* **1999**, *8*, 382−390.
(40) Todd, B. D.; Evans, D. J. *J. Chem. Phys.* **1995**, *103*, 9804−9809.
(41) Travis, K. P.; Gubbins, K. E. *J. Chem. Phys.* **2000**, *112*, 1984−1994.
(42) Kong, Y.; Manke, C. W.; Madden, W. G.; Schlijper, A. G. *Int. J. Thermophys.* **1994**, *15*, 1093−1101.
(43) Jones, J. L.; Lal, M.; Ruddock, J. N.; Spenley, N. A. *Faraday Discuss.* **1999**, *112*, 129−142.
(44) Revenga, M.; Zuniga, I.; Espanol, P. *Comput. Phys. Commun.* **1999**, *121*, 309−311.
(45) Fan, X. J.; Phan-Thien, N.; Yong, N. T.; Wu, X. H.; Xu, D. *Phys. Fluids* **2003**, *15*, 11−21.
(46) Willemsen, S. M.; Hoefsloot, H. C. J.; Iedema, P. D. *Int. J. Mod. Phys. C* **2000**, *11*, 881−890.
(47) Toutain, P. L. *AAPS PharmSci (http://www.aapspharmsci.org)* **2002**, *4*, Article 38.
(48) de Gennes, P. G. *Macromolecules* **1980**, *13*, 1069−1075.
(49) Iwata, H.; Hirata, I.; Ikada, Y. *Macromolecules* **1998**, *31*, 3671−3678.
(50) Clement, F.; Charitat, T.; Johner, A.; Joanny, J.-F. *Europhys. Lett.* **2001**, *54*, 65−71.
(51) Doyle, P. S.; Shaqfeh, E. S. G.; Gast, A. P. *Macromolecules* **1998**, *31*, 5474−5486.
(52) Saphiannikova, M. G.; Pryamitsyn, V. A.; Cosgrove, T. *Macromolecules* **1998**, *31*, 6662−6668.
(53) Ivkov, R.; Butler, P. D.; Satija, S. K.; Fetters, L. J. *Langmuir* **2001**, *17*, 2999−3005.
(54) Castro, R. P.; Monbouquette, H. G.; Cohen, Y. *J. Membr. Sci.* **2000**, *179*, 207−220.

MA060628F